Part Two
Model Systems with Stress-Engineered Properties

Mechanical Stress on the Nanoscale: Simulation, Material Systems and Characterization Techniques, First Edition.
Edited by Margrit Hanbücken, Pierre Müller, and Ralf B. Wehrspohn.

5
Accommodation of Lattice Misfit in Semiconductor Heterostructure Nanowires

Volker Schmidt and Joerg V. Wittemann

5.1
Introduction

By far the most important trait of semiconductor nanowires is that, relative to their volume, they have a large surface. Many essential properties, such as the thermodynamics of growth or the electrical properties, are affected by the presence and the quality of the nanowire surface [1]. With the surface area to volume ratio being inversely proportional to the nanowire diameter, the physical properties of nanowires are naturally more severely affected when the nanowire is thinner. The fact that nanowires possess a large free surface also has substantial influence on their mechanical properties, in particular considering heterostructure nanowires combining materials with different lattice constants. The coherent epitaxial growth of such two materials would cause one or both materials to be strained by the misfit. What makes misfit-strained heterostructure nanowires such appealing objects is that contrary to heteroepitaxial layers on planar substrates, which cannot expand or shrink in lateral direction, a nanowire possesses a free surface that can adjust according to the strain within it. By changing its diameter and—suppose that the nanowire has a free end—also its lengths, a heterostructure nanowire can elastically relax a part of the strain energy induced by the misfit. Owing to its enhanced possibilities for partial elastic relaxation, the onset of other strain relaxation mechanisms such as dislocation formation or a roughening of the surface can be suppressed or at least deferred. It will be shown in the following to which extend this is indeed the case.

Generally, one can distinguish between two main types of nanowire heterostructures: (a) axial heterostructures, in which cylindrical pieces of distinct materials contact each other with their flat ends, creating a circular interface and (b) core–shell heterostructures, in which a cylindrical piece of one material is radially enwrapped by the second material. Both types, axial heterostructures and core–shell nanowire heterostructures, have been experimentally realized [2–9].

In addition to these two types of heterostructures, there are two main strain relaxation mechanisms that are usually tried to be avoided. The first is dislocation formation. Besides destroying the coherency of the heterostructure interface,

Mechanical Stress on the Nanoscale: Simulation, Material Systems and Characterization Techniques, First Edition. Edited by Margrit Hanbücken, Pierre Müller, and Ralf B. Wehrspohn.

dislocations may have a negative influence on the electrical properties of the nanowires due to carrier recombination at the dislocation core. Another reason why dislocation formation is mostly undesired is that the misfit strain affects the band structure alignment of the materials of which the heterostructure is composed. Dislocations now locally render the strain field, so the band structure alignment is also disturbed.

The second basic mechanism by which a misfit-strained layer or structure can relieve part of the strain energy is through surface roughening. During the growth of a strained layer on a substrate of a different lattice constant, the layer is inherently unstable with respect to modulations of the growing surface. The reason for this is that the overall strain energy of a system having a strained but undulated surface is smaller compared to a system with a flat and coherently strained layer; and this reduction in strain energy is what is driving the instability. Ultimately, this instability, the so-called Asaro–Tiller–Grinfeld instability [10, 11], may lead to the formation of clusters on the surface (see Figure 5.1c). This effect is also employed for the self-organized synthesis of quantum dots, and in this context it has received considerable attention in the past (see, for example, the excellent review by Stangl *et al.* [12] and references therein). Concerning the synthesis of heterostructure nanowires, this instability of the surface is rather thought of as a nuisance than as an advantage, as it would prevent the synthesis of heterostructure nanowires strained in a well-defined manner.

For clarity, the two strain relaxation mechanisms (dislocation formation and roughening) are separately dealt with. Applied to the two main types of heterostructures (axial and core–shell), this leaves us with four separate scenarios. However, as strain-induced roughening during the synthesis of axial heterostructures completely prevents the synthesis of an axial nanowire heterostructure, this possible scenario is not considered. First, we will take a look at dislocation formation in axial heterostructure nanowires in the following section, as schematically indicated in

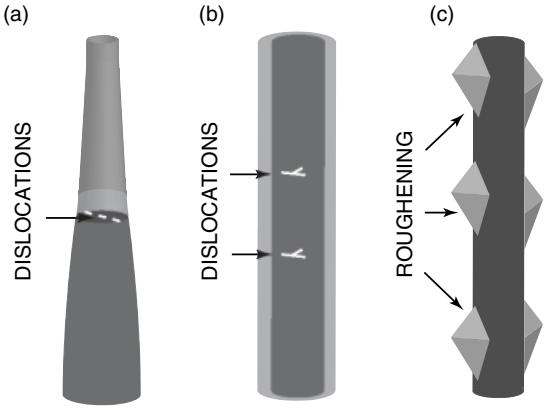

Figure 5.1 The different strain relaxation scenarios. (a) Dislocation formation in case of axial heterostructure nanowires. (b) Dislocation formation in core–shell nanowires. (c) Roughening of the shell in case of core–shell nanowires.

Figure 5.1a, then dislocation formation in core–shell nanowires (Figure 5.1b) will be discussed, and finally surface roughening of core–shell nanowire heterostructures will be considered.

5.2
Dislocations in Axial Heterostructure Nanowires

As already mentioned, the two main strain relaxation mechanisms are the formation of dislocations and the roughening of the surface. Considering the growth of strained layers on planar substrates, Tersoff and LeGoues [13] could elegantly show that the interplay of these two relaxation mechanisms is such that at small lattice misfits the formation of dislocations is favored, whereas large misfits rather promote a roughening of the surface. In the latter case, this does not exclude that dislocations will be formed, but a roughening of the surface would still precede the formation of dislocations. In the following, we will always refer to a roughening of the surface, even if island formation would in some cases be the more appropriate description of the surface morphology. Concerning the growth of axial heterostructure nanowires, it should be mentioned that these nanowires are in most cases synthesized by the vapor–liquid–solid [14] mechanism. This means that a liquid catalyst droplet promotes the growth of nanowires by acting as a preferential site for adsorption of precursor molecules from the gas phase, supplying the semiconductor material. The balance of such a liquid catalyst droplet at the nanowire tip is delicate. Changes in the growth parameters, for example, can easily lead to a kinking of the nanowires. A roughening of the catalyst–nanowire interface presumably perturbs the growth of nanowire to such an extent that a well-defined synthesis cannot take place anymore. A roughening of the catalyst–nanowire interface, therefore, has to be prevented at all costs. Since there are presently to best of our knowledge no experimental studies on the interplay of the vapor–liquid–solid mechanism with a potential roughening of the catalyst–droplet interface, this problem will not be considered. Still, one should be aware that in particular for the synthesis of axial nanowire heterostructure with large lattice misfit, interface roughening might turn out to be a serious obstacle. Instead, we concentrate in this section on dislocation formation, keeping in mind that according to the analysis of Tersoff and LeGoues [13], dislocation formation is the more critical mechanism at smaller misfits.

The analysis presented in this section closely follows the work of Ertekin *et al.* [15], who at first recognized the potential of nanowires for the synthesis of dislocation-free strained heterostructures. In fact, the calculation presented represents a simplified version of Ertekin's work, assuming equal Young's modulus E and Poison ratio ν for both materials. The system considered is a single nanowire heterostructure interface (cf. Figure 5.1a) with the two materials having a (positive) misfit m. The two material segments are assumed to have infinite length and a common equilibrium radius R at infinite distance from the interface. That means that the relative difference in radius, which is equal to the misfit, is neglected in the analysis as it would render the outcome only slightly. Considering only the radial component of the strain tensor

(in cylindrical coordinates), the strain energy density, en, at the interface is given by

$$\mathrm{en} = \left(\frac{E}{1-\nu}\right)\frac{m^2}{4} \tag{5.1}$$

Ertekin *et al.* [15] assumed that the strain energy density decays exponentially with the distance from the interface and that the characteristic length for this exponential decay is equal to $\alpha \times R$. They found that $\alpha = 0.1875$ indeed describes the behavior well. Integrating over the length of the nanowire, the total strain energy En_0 stored in a dislocation-free nanowire is then given by

$$\mathrm{En}_0 = \frac{\alpha\pi R^3}{2}\left(\frac{E}{1-\nu}\right)m^2 \tag{5.2}$$

In a rather crude approximation, it is assumed that the formation of a dislocation reduces the misfit to

$$m_{\mathrm{eff}} = m - \frac{b}{2R} \tag{5.3}$$

with b being Burger's vector of the dislocation. In addition to reducing the strain energy of the system by reducing the misfit, the intrinsic energy of the dislocation, that is, the energy of the dislocation core and the strain field of dislocation, should be taken into account. Taking R and $b/4$ as the upper and inner cutoff limits for the strain field of the dislocation and accounting for the reduced effective misfit, the strain energy of a nanowire having a single dislocation at the interface can be approximated as

$$\mathrm{En}_1 = \frac{\alpha\pi R^3}{2}\left(\frac{E}{1-\nu}\right)\left(m - \frac{b}{2R}\right)^2 + \frac{Rb^2}{2\pi(1+\nu)}\left(\frac{E}{1-\nu}\right)\log\left(\frac{4R}{b}\right) \tag{5.4}$$

If it is further assumed that dislocations are only introduced once it turns out to be energetically favorable; that is, if the energy En_1 is smaller than En_0, a criterion for a critical misfit m_{crit} can be derived by equating Eqs (5.3) and (5.4). One can easily find that

$$m_{\mathrm{crit}} = \frac{b}{4R} + \frac{b}{\alpha\pi^2 R(1+\nu)}\log\left[\frac{4R}{b}\right] \tag{5.5}$$

Note that the critical misfit does not depend on Young's modulus E of materials. This model, based on energetic considerations, neglects several important aspects such as dislocation nucleation and gliding of dislocations, and the outcome therefore should be considered as a rough estimate of the onset of dislocation formation. A calculation on dislocation formation in axial nanowires in which nucleation aspects are taken into account has been performed by Kästner and Gösele [16]. Although their result differs from the one of Ertekin *et al.* [15], the general diameter-dependent behavior is similar. The critical misfit m_{crit}, according to Eq. (5.5), at which the formation of dislocations should set in is shown in Figure 5.2 as a function of the nanowire diameter $2R$, assuming a Burger's vector $b = 0.3$ nm. As long as the misfit

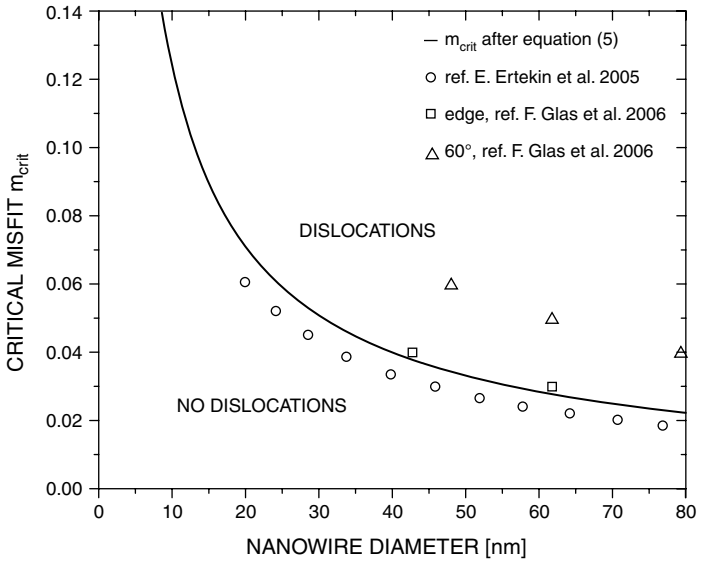

Figure 5.2 Critical misfit m_{crit} for $b = 0.30$ nm and $\nu = 0.25$ using Eq. (5.5). As reference, the data of Ertekin *et al.* [17] (○) and Glas [18] △, □) are shown.

m at a certain radius does not exceed the critical misfit m_{crit}, the nanowire heterostructure interface should remain dislocation free.

One can see in Figure 5.2 that the critical misfit, at which the formation of dislocation should theoretically set in, is quite substantial. At the nanowire diameter of 35 nm, the critical misfit is already 4.5%, which should theoretically suffice to synthesize dislocation-free Si–Ge heterostructure nanowires, and owing to the dominant $1/R$ dependence, the critical misfit becomes huge for even smaller diameters. Since the calculation presented presumably oversimplifies the complexity of the real situation, the outcomes of the more elaborate calculations of Ertekin *et al.* [17] and Glas [18] (considering both edge and 60° dislocations) are also shown as reference. In particular, the data for 60° dislocation seem to be in reasonable agreement with experimental observations [18], so one may conclude that the critical misfit as given by Eq. (5.5) rather underestimates the true value.

5.3
Dislocations in Core–Shell Heterostructure Nanowires

Synthesizing dislocation-free core–shell nanowires in which the shell material has a large misfit with respect to the core is an interesting task because one can in principle achieve very high strains in the material, in particular in the core. Such high strains could induce changes in the band structure, which is appealing from an electronics device point of view as it may increase the charge carrier mobility [19]. In the case of a

core–shell structure, such a mobility increase could be further enhanced by carefully adjusting the core–shell band alignment and the doping profile [8], which together with the possibility of realizing a surround-gate architecture [20] could be an interesting approach to high performance devices. Yet, there are two main obstacles that need to be overcome, and these are the formation of dislocations and the roughening of the shell. The point at issue is whether, and for which parameters, the onset of these two strain relaxation mechanisms can be avoided or suppressed for such a strained core–shell nanostructure. In this section, the question of dislocation formation will be discussed following the work of Liang *et al.* [21].

Let us consider a core–shell heterostructure nanowire as shown in Figure 5.1b, having a core radius R_1, a shell radius R_2, and a misfit m at the core–shell interface. Liang *et al.* [21] investigated the effect of two different types of dislocations: edge dislocations and dislocation loops. They found that dislocation loops are less critical than edge dislocations; we concentrate here on the latter case. According to their calculation, the formation of an edge dislocation reduces the strain energy stored in the core–shell system by an amount

$$\Delta \mathrm{En} = \frac{bGm(1+\nu)R_1(R_2^2-R_1^2)}{(1-\nu)R_2^2} \tag{5.6}$$

with $G = E/2(1+\nu)$ being the shear modulus and ν the Poisson ratio. Both constants are assumed to be the same for the core and shell materials, respectively. Furthermore, Liang *et al.* [21] approximate the energy of the edge dislocation as

$$\mathrm{En}_{\mathrm{dis}} = \frac{b^2 G}{4\pi(1-\nu)}\left(\ln\left[\frac{R_2^2-R_1^2}{R_2 r_c}\right] + \left(\frac{R_1}{R_2}\right)^2 - \frac{3}{2}\right) \tag{5.7}$$

where b again denotes Burger's vector of the dislocation and r_c is the inner cutoff of the dislocation strain field. Equations (5.6) and (5.7) then directly lead to the critical misfit that the core–shell system can sustain without forming edge dislocations.

$$m_{\mathrm{crit}} = \frac{bR_2^2}{4\pi(1+\nu)R_1(R_2^2-R_1^2)}\left(\ln\left[\frac{R_2^2-R_1^2}{R_2 r_c}\right] + \left(\frac{R_1}{R_2}\right)^2 - \frac{3}{2}\right) \tag{5.8}$$

Note that similar to (5.5), Eq. (5.8) does not depend on the shear modulus of the materials involved. For a Burger's vector of $b = 0.3$ nm and an inner cutoff radius $r_c = b/4$, the critical misfit m_{crit} according to Eq. (5.8) is shown in Figure 5.3a as a function of the shell thickness for various core radii R_1.

As long as the misfit m is smaller than the value given for a specific shell thickness and core radius, the system should remain dislocation free. Considering the curve for $R_1 = 5$ nm, one can see that m_{crit} decreases with increasing shell thickness until it reaches a minimum value (about 0.016) at a shell thickness of about 10 nm. Thus, if shell thicknesses of less than 10 nm are aimed at, a misfit larger than 0.016 would be tolerated by the system without forming edge dislocations. If, however, the intended shell thickness is larger than 10 nm, it is necessary that the misfit be chosen below the minimum value. At a misfit smaller than the value at the minimum, the system will

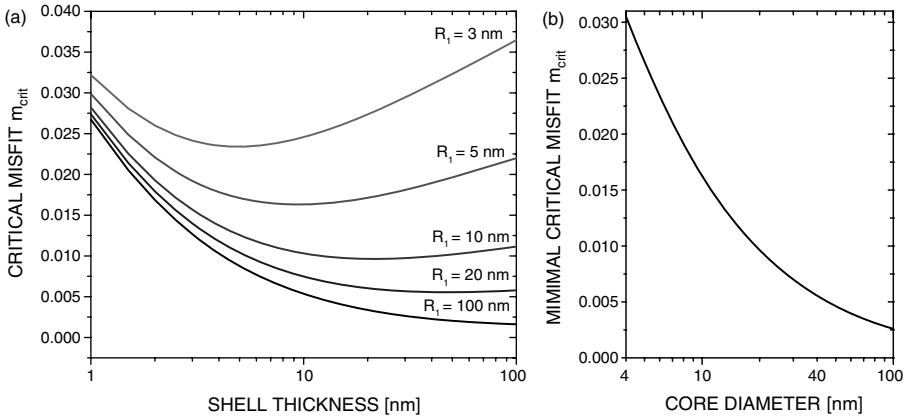

Figure 5.3 (a) Critical misfit m_{crit} that a core–shell nanowire can sustain without forming edge dislocations given here as a function of the shell thickness for various core radii R_1. The Burger vector b is taken to be 0.3 nm and $r_c = b/4$. (b) Critical misfit at the minimum of m_{crit} (as shown in (a)) as a function of the core diameter.

not tend to form dislocations, irrespective of the shell thickness. Therefore, it is instructive to take a look at how this minimum of m_{crit} behaves as a function of the core diameter $2R_1$. This is shown in Figure 5.3b. As one can see in this graph, the minimum of m_{crit} is strongly diameter dependent and increases to a value of about 0.03 at a core diameter of 4 nm. This outcome is somehow similar to that presented in the previous section, in the sense that reducing the diameter shifts the misfit limit for dislocation formation to greater values. Thus, reducing the diameter is advisable when dislocations in core–shell nanowires are to be prevented.

5.4
Roughening of Core–Shell Heterostructure Nanowires

The second major obstacle that complicates the synthesis of misfit-strained core–-shell nanowires is the potential roughening of the shell. During the growth of the shell, the system tends to partially relax strain by developing a modulation of the surface. This may in the end lead to the creation of islands or notches on the surface, as schematically indicated in Figure 5.1c. As already mentioned, this relaxation mechanism can be expected to be particularly critical at large misfit strains [13]. The creation of islands or notches is caused by the so-called Asaro–Tiller–Grinfeld instability [10, 11], a strain-induced morphological instability of the surface. The driving force for this instability is that an undulation of the surface leads to a redistribution of the strain energy, such that it reduces the overall strain energy of the system. On the other hand, this surface waviness comes with an increase in the overall surface area. Nevertheless, for some types of modulations, the energetic costs of increasing the surface area are smaller than the gain of reducing the elastic energy,

so the growth of a modulated surface is energetically favored. For the growth of strained films on planar substrates, this instability has been the subject of extensive investigations [22–25]. However, these results may not be directly applicable to misfit-strained core–shell nanowires, as a bulk substrate is much less susceptible to a strained layer than a nanowire. For a misfit-strained core–shell nanowire, one can expect that a large portion of the elastic energy is stored in the core, whereas in case of a bulk substrate, it is the strained film that basically contains the whole elastic energy.

In this section, the misfit-driven morphological instability of core–shell nanowires is analyzed by performing a linear stability analysis, closely following the work of Schmidt *et al.* [26]. Instead of assuming unidirectional stress along the centerline of the wire [27, 28], the misfit at the interface will be properly accounted. Furthermore, nonradially symmetric modulations will also be taken into account, which is necessary as the presence of islands usually breaks axial symmetry [29]. As pointed out previously, the effects of surface stress on the instability are consistently incorporated into the model.

The system under consideration is a cylindrical, completely dislocation-free, core–shell nanowire. The shell material has a misfit m with respect to the core that causes both core and shell to be elastically strained. For simplicity, the shear modulus G, the Poisson ratio ν, the surface stress τ, and the surface free energy γ are taken to be isotropic quantities. The linear stability analysis follows the works of Mullins [30] and Spencer *et al.* [25]. The idea behind it is that a core–shell nanowire in reality is not perfectly cylindrical; instead, it will show local deviations of cylindrical geometry. These local deviations can be also described by a broad distribution of sinusoidal surface modulations characterized by their wavenumber q in axial direction (the $\hat{\mathbf{z}}$-direction) and the mode number n in circumferential direction. Thus, if the outer radius of the unperturbed core–shell nanowire is R_2 and δ is the amplitude of the perturbation, then the actual surface radius R_s can be expressed as

$$R_s = R_2 + \delta \cos(qz)\cos(n\phi) \tag{5.9}$$

These modulations or perturbations of the shell thickness change the strain energy distribution that in turn leads to a variation in the chemical potential at the nanowire surface. The inhomogeneity of the chemical potential can drive surface diffusion, leading to an increase or decrease of the initial perturbation amplitude. In this way, a positive or negative feedback is created; the question arises whether there are modes for which a positive feedback exists (i.e., perturbations that exponentially increase in amplitude), what characteristics these modes have, and how different parameters such as the misfit m or the core radius R_1 affect the stability of the system with respect to the growth of these modes.

To answer this question, first one should figure out how the strain distribution changes as a consequence of a surface modulation of amplitude δ. This is done perturbatively by analytically calculating the stress and strain distributions to first order in δ. After some definitions, the zeroth order, that is, the stress/strain distribution of a perfectly cylindrical misfit-strained core–shell nanowire, is calculated. All corresponding zeroth-order quantities, such as the displacement $\bar{\nu}_i$, the

strain $\bar{u}_{ij}$, the elastic strain $\bar{\varepsilon}_{ij}$, or the stress $\bar{\sigma}_{ij}$, are marked by an overbar. In the following section, the first-order changes to the stress/strain distribution are determined. All first-order contributions are marked by a tilde. Furthermore, for brevity, an index α is introduced, which is equal to 1 if a quantity refers to the nanowire core and 2 for a corresponding shell quantity.

5.4.1 Zeroth-Order Stress and Strain

To determine the zeroth stress/strain distribution, we assume that the system is in equilibrium, which means that in the absence of external body forces, the displacement vector u has to fulfill the equations of equilibrium [31]

$$(1-2\nu)\Delta\mathbf{u} + \nabla(\nabla\cdot\mathbf{u}) = 0 \tag{5.10}$$

By solving the above equations and imposing proper boundary conditions, one can arrive at an analytical solution for the displacement vector $\mathbf{u}$. Using cylindrical coordinates, that is, $\mathbf{u} = u_r\hat{\mathbf{r}} + u_\phi\hat{\phi} + u_z\hat{\mathbf{z}}$, the strain tensor u_{ij} can be derived from the displacement vector $\mathbf{u}$ [31]:

$$u_{rr} = \partial_r u_r \tag{5.11}$$

$$u_{zz} = \partial_z u_z \tag{5.12}$$

$$u_{\phi\phi} = r^{-1}\partial_\phi u_\phi + r^{-1}u_r \tag{5.13}$$

$$u_{rz} = (\partial_z u_r + \partial_r u_z)/2 \tag{5.14}$$

$$u_{\phi z} = (r^{-1}\partial_\phi u_z + \partial_z u_\phi)/2 \tag{5.15}$$

$$u_{r\phi} = (\partial_r u_\phi - r^{-1}u_\phi + r^{-1}\partial_\phi u_r)/2 \tag{5.16}$$

These equations are analogously valid for the zeroth- and first-order quantities $\bar{u}_{ij}$ and $\tilde{u}_{ij}$, respectively. To account for the lattice misfit m defined as

$$m = \frac{l_2 - l_1}{l_1} \tag{5.17}$$

with l_1 and l_2 being the lattice constants of the core and the shell, respectively, it is necessary to introduce the elastic strain tensor ε_{ij}.

$$\varepsilon_{ij}^{\alpha} = u_{ij}^{\alpha} - m\delta_{ij}\delta_{\alpha 2} \tag{5.18}$$

with δ_{ij} and $\delta_{\alpha 2}$ being Kronecker deltas. The idea behind introducing this additional tensor is that one can elegantly incorporate the misfit into the calculation this way. It is the elastic strain tensor ε_{ij} that reflects the strain in the core–shell system. According to the above definition, compressive stresses/strains are negative

and tensile stresses/strains are positive. From the elastic strain tensor, one can then obtain the stress tensor [31]

$$\sigma_{ij}^{\alpha} = \frac{2G_{\alpha}}{1-2\nu_{\alpha}}\left((1-2\nu_{\alpha})\varepsilon_{ij}^{\alpha} + \nu_{\alpha}\varepsilon_{ll}^{\alpha}\delta_{ij}\right) \tag{5.19}$$

with G_{α} being the shear modulus and ν_{α} the Poisson ratio of the core or shell. Together with Eq. (5.18), this leads to the following relation:

$$\sigma_{ij}^{\alpha} = \frac{2G_{\alpha}}{1-2\nu_{\alpha}}\left((1-2\nu_{\alpha})u_{ij}^{\alpha} + \nu_{\alpha}u_{ll}^{\alpha}\delta_{ij} - (1+\nu_{\alpha})m\delta_{ij}\delta_{\alpha 2}\right) \tag{5.20}$$

Similar relations hold for the zeroth-order quantities

$$\bar{\varepsilon}_{ij}^{\alpha} = \bar{u}_{ij}^{\alpha} - m\delta_{ij}\delta_{\alpha 2} \tag{5.21}$$

$$\bar{\sigma}_{ij}^{\alpha} = \frac{2G_{\alpha}}{1-2\nu_{\alpha}}\left((1-2\nu_{\alpha})\bar{u}_{ij}^{\alpha} + \nu_{\alpha}\bar{u}_{ll}^{\alpha}\delta_{ij} - (1+\nu_{\alpha})m\delta_{ij}\delta_{\alpha 2}\right) \tag{5.22}$$

and to the first-order contributions

$$\tilde{\varepsilon}_{ij}^{\alpha} = \tilde{u}_{ij}^{\alpha} \tag{5.23}$$

$$\tilde{\sigma}_{ij}^{\alpha} = \frac{2G_{\alpha}}{1-2\nu_{\alpha}}\left((1-2\nu_{\alpha})\tilde{u}_{ij}^{\alpha} + \nu_{\alpha}\tilde{u}_{ll}^{\alpha}\delta_{ij}\right) \tag{5.24}$$

Let us come back now to the task of calculating the stress/strain distribution of an unperturbed, perfectly cylindrical, misfit-strained core–shell nanowire. Owing to radial symmetry and translational invariance with respect to translations in $\hat{\mathbf{z}}$-direction, the equations of equilibrium (5.10) reduce to

$$\partial_r^2\bar{u}_r^{\alpha} + \frac{1}{r}\partial_r\bar{u}_r^{\alpha} - \frac{1}{r^2}\bar{u}_r^{\alpha} = 0 \tag{5.25}$$

$$\partial_z^2\bar{u}_z^{\alpha} = 0 \tag{5.26}$$

with the corresponding solutions

$$\bar{u}_r^{\alpha} = a_{\alpha}r + b_{\alpha}\frac{1}{r} \tag{5.27}$$

$$\bar{u}_z^{\alpha} = c_{\alpha}z \tag{5.28}$$

where a_{α}, b_{α}, and c_{α} are six so far undetermined constants—or better five unknown constants as b_1 has to be equal to zero to obtain solutions that are finite at $r = 0$. The remaining unknown constants (a_1, a_2, b_2, c_1, c_2) can be determined by imposing proper boundary conditions.

As already mentioned, surface effects play a crucial role in the physics and properties of nanowires. Considering the elastic properties of nanowires, surface stress needs to be considered, in particular if nanowires of very small radius are taken into account. But one should be careful not to mix up surface stresses with surface

free energies because, as first pointed out by Gibbs [32], the surface free energy γ of a solid does not necessarily equal the surface stress τ (see, for example, the work of Shuttleworth [33]). The difference between these two quantities is that the surface free energy γ is related to the work of creating new area, for example, by splitting or dewetting, whereas the surface stress τ is related to the work of increasing the surface area by elastically deforming the solid [34]. In general, this deformation work should be characterized by introducing a second-rank tensor τ_{ij}, the so-called surface stress tensor. For isotropic surfaces, however, this tensor $\tau_{ij} = \tau\delta_{ij}$ reduces to a scalar, the surface stress τ. To find a reasonable estimate for the magnitude of τ turns out to be difficult as the surface stresses often exhibit a pronounced anisotropy [35–37], depend on the type of surface reconstruction [38–41], and are furthermore altered by the presence of adatoms [42, 43]. Surface stress values, for example, calculated by Meade and Vanderbilt [42] for a Si(111) surface, range from -0.7 to 2.4 N/m depending on the specific surface configuration. In view of these ambiguities, a surface stress value of $\tau = 1$ N/m will be used in the course of the calculation. This seems a fair estimate considering the values given in Refs [38–43].

One of the boundary conditions to be imposed is that there are no net forces acting normal to the surface. Including the effect of surface stress, this corresponds to

$$\sigma_{ij}n_j + P^{\mathrm{f}}n_i + \tau\kappa n_i = 0 \tag{5.29}$$

with P^{f} being the pressure in the surrounding fluid, n_j the outward-pointing surface normal, τ the surface stress, and κ the sum of the principle curvatures of the surface. In our case, we can neglect the pressure P^{f} of the surrounding fluid as it is typically orders of magnitude too small to affect the elasticity problem. The boundary conditions to be imposed are as follows [26]:

1) Equal displacements at the core–shell interface (coherent interface), which gives

$$\bar{u}_r^{(1)}|_{R_1} = \bar{u}_r^{(2)}|_{R_1} \text{ and } \bar{u}_z^{(1)}|_{R_1} = \bar{u}_z^{(2)}|_{R_1}$$

2) Zero net normal force at the core–shell interface. With the outward normal $\bar{n}_j^{(1)} = \hat{\mathbf{r}}$ of the core–shell interface, this leads to

$$\bar{\sigma}_{rr}^{(1)}|_{R_1} = \bar{\sigma}_{rr}^{(2)}|_{R_1}$$

3) Zero net force in $\hat{\mathbf{z}}$-direction. Considering the force is created by the surface stress leads to

$$R_1^2\bar{\sigma}_{zz}^{(1)} + (R_2^2 - R_1^2)\bar{\sigma}_{zz}^{(2)} = -2\tau R_2$$

4) Zero net normal force at the surface. With $\bar{n}_j^{(2)} = \hat{\mathbf{r}}$, this gives

$$\bar{\sigma}_{rr}^{(2)}|_{R_2} = -\frac{\tau}{R_2}$$

If it is further assumed that core and shell have the same shear modulus and Poisson ratio, that is, $G_1 = G_2 = G$ and $\nu_1 = \nu_2 = \nu$, the five unknown constants become

$$a_1 = \frac{m(1-3\nu)(R_2^2-R_1^2)}{2(1-\nu)R_2^2} - \frac{\tau(1-3\nu)}{2G(1+\nu)R_2} \tag{5.30}$$

$$a_2 = \frac{m(2R_2^2(1-\nu)-R_1^2(1-3\nu))}{2(1-\nu)R_2^2} - \frac{\tau(1-3\nu)}{2G(1+\nu)R_2} \tag{5.31}$$

$$b_1 = 0 \tag{5.32}$$

$$b_2 = \frac{-m(1+\nu)R_1^2}{2(1-\nu)} \tag{5.33}$$

$$c_1 = \frac{m(R_2^2-R_1^2)}{R_2^2} - \frac{\tau(1-\nu)}{G(1+\nu)R_2} \tag{5.34}$$

$$c_2 = c_1 \tag{5.35}$$

Using Eqs (5.27–5.28), one can derive the displacements $\bar{u}_r$ and $\bar{u}_z$, which then leads to the strain tensor $\bar{u}_{ij}$ (using (5.11–5.16), the elastic strain tensor $\bar{\varepsilon}_{ij}$ (using (5.21)), and the stress tensor $\bar{\sigma}_{ij}$ (using (5.22)).

5.4.2
First-Order Contribution to Stress and Strain

Let us now examine how adding a sinusoidal perturbation changes the stress/strain distribution. To arrive at expressions for the first-order contributions $\tilde{\varepsilon}_{ij}$ or $\tilde{\sigma}_{ij}$ is, in principle, straightforward; instead of solving the equations of equilibrium (5.10) for the displacement vector, they are solved for the so-called Papkovich–Neuber potentials [44, 45] Ψ and ξ, with $\Psi = \Psi_r\hat{\mathbf{r}} + \Psi_\phi\hat{\phi} + \Psi_z\hat{\mathbf{z}}$ being a vector potential and ξ being a scalar potential. From the Papkovich–Neuber potentials, one can then derive the displacement using the following relation [46]:

$$\mathbf{u} = 4(1-\nu)\Psi - \nabla(\mathbf{R}\cdot\Psi + \xi) \tag{5.36}$$

with $\mathbf{R} = r\hat{\mathbf{r}} + z\hat{\mathbf{z}}$. The main advantage of the Papkovich–Neuber potentials is that they reduce the equations of equilibrium (5.10) to independent Laplace's equations

$$\Delta\cdot\Psi = 0 \tag{5.37}$$

$$\Delta\xi = 0 \tag{5.38}$$

Considering radial symmetry, the corresponding solutions are easily found:

$$\xi^\alpha = [d_\alpha\mathcal{I}_n(qr) + e_\alpha\mathcal{K}_n(qr)]\cos(qz)\cos(n\phi) \tag{5.39}$$

$$\begin{aligned}\psi_r^\alpha = [&f_\alpha\mathcal{I}_{n+1}(qr) + g_\alpha\mathcal{I}_{n-1}(qr) + h_\alpha\mathcal{K}_{n+1}(qr)\\ &+ i_\alpha\mathcal{K}_{n-1}(qr)]\cos(qz)\cos(n\phi)\end{aligned} \tag{5.40}$$

$$\psi_{\phi}^{\alpha} = [f_{\alpha}\mathcal{I}_{n+1}(qr) - g_{\alpha}\mathcal{I}_{n-1}(qr) + h_{\alpha}\mathcal{K}_{n+1}(qr) - i_{\alpha}\mathcal{K}_{n-1}(qr)]\cos(qz)\sin(n\phi) \tag{5.41}$$

$$\psi_{z}^{\alpha} = [j_{\alpha}\mathcal{I}_{n}(qr) + k_{\alpha}\mathcal{K}_{n}(qr)]\cos(qz)\cos(n\phi) \tag{5.42}$$

with $\mathcal{I}_n(qr)$ and $\mathcal{K}_n(qr)$ being the modified Bessel functions of order n. The values of the constants d_α, e_α, f_α, g_α, h_α, i_α, j_α, and k_α should be determined by imposing boundary conditions. Three of these constants can be found directly. By demanding that the solution has to be finite at $r = 0$, the constants e_1, h_1, and i_1 have to be equal to zero.

Moreover, it turns out to be useful to introduce the normal vectors $\tilde{n}_i^{(1)}$ and $\tilde{n}_i^{(2)}$ of the core–shell interface and the surface, respectively. The core is assumed to be cylindrical, so that $\tilde{\mathbf{n}}^{(1)} = \hat{\mathbf{r}}$. The normal to the outer surface $\tilde{\mathbf{n}}^{(2)} = \hat{\mathbf{r}} + \eta_\phi\hat{\phi} + \eta_z\hat{\mathbf{z}}$, with

$$\eta_{\phi} = \delta\frac{n}{R_2}\cos(qz)\sin(n\phi) \tag{5.43}$$

$$\eta_{z} = \delta q\sin(qz)\cos(n\phi) \tag{5.44}$$

Moreover, the curvature κ of the nanowire surface is

$$\kappa = \frac{1}{R_2} + \delta\left(\frac{n^2-1}{R_2^2} + q^2\right)\cos(qz)\cos(n\phi) \tag{5.45}$$

With this, the boundary conditions then become

1) Equality of displacements at the core–shell interface, leading to

$$\tilde{u}_r^{(1)}|_{R_1} = \tilde{u}_r^{(2)}|_{R_1}$$
$$\tilde{u}_z^{(1)}|_{R_1} = \tilde{u}_z^{(2)}|_{R_1}$$
$$\tilde{u}_\phi^{(1)}|_{R_1} = \tilde{u}_\phi^{(2)}|_{R_1}$$

2) Zero net normal force at the core–shell interface. This gives three conditions:

$$\tilde{\sigma}_{rr}^{(1)}|_{R_1} = \tilde{\sigma}_{rr}^{(2)}|_{R_1}$$
$$\tilde{\sigma}_{r\phi}^{(1)}|_{R_1} = \tilde{\sigma}_{r\phi}^{(2)}|_{R_1}$$
$$\tilde{\sigma}_{rz}^{(1)}|_{R_1} = \tilde{\sigma}_{rz}^{(2)}|_{R_1}$$

3) Zero net normal force at the surface:

$$\sigma_{ij}^{(2)}\tilde{n}_j^{(2)}|_{r=R_2} = -\tilde{n}_i^{(2)}\tau\kappa$$

This finally leads to the last three conditions

$$\tilde{\sigma}_{rr}^{(2)}|_{R_2} = -\delta\tau\left(q^2 + \frac{n^2-1}{R_2}\right)\cos(qz)\cos(n\phi)$$

$$\tilde{\sigma}_{r\phi}^{(2)}|_{R_2} = -\delta\frac{n}{R_2}\left(\bar{\sigma}_{\phi\phi}^{(2)}|_{R_2} + \frac{\tau}{R_2}\right)\cos(qz)\sin(n\phi)$$

$$\tilde{\sigma}_{zr}^{(2)}|_{R_2} = -\delta q\left(\bar{\sigma}_{zz}^{(2)}|_{R_2} + \frac{\tau}{R_2}\right)\sin(qz)\cos(n\phi)$$

This set of equations can be solved for the nine unknown constants, which is simplified by the fact that for $G_1 = G_2 = G$ and $\nu_1 = \nu_2 = G$, the boundary conditions are fulfilled if $e_2 = h_2 = i_2 = 0$, $d_1 = d_2, f_1 = f_2$, and $g_1 = g_2$. Thus, in this case, it suffices to determine d_2, g_2, and h_2. Having these expressions at hand, one can then determine the Papkovich–Neuber potentials, derive the displacement, and from the displacement the strain, the elastic strain, and the stress. These first-order contributions can then be combined with the corresponding zeroth-order results to obtain the full stress and strain distributions to first order in δ.

5.4.3
Linear Stability Analysis

Having calculated the stress/strain distribution to first order in δ for an arbitrary surface perturbation, defined by its wavenumber q and its mode number n, one has to determine how surface diffusion affects the amplitude of the perturbation, that is, to figure out whether surface diffusion amplifies or attenuates a specific perturbation. Following the work of Spencer *et al.* [24], the diffusion-induced surface flux J_s can be expressed as [47–49]

$$J_s = \frac{-D_s\Gamma}{kT}\nabla_s M_\nu \tag{5.46}$$

with D_s being the surface diffusion constant, Γ the area density of lattice sites, and ∇_s the surface gradient; kT has its usual meaning and the diffusion potential, M_ν, is given by [24]

$$M_\nu = \Omega\left(\gamma\kappa + \frac{1}{2}\sigma_{ij}\varepsilon_{ij}\right)_{r=R_s} \tag{5.47}$$

where γ is the surface energy density, κ the curvature of the strained system, and Ω the volume per atom. The $(1/2)\sigma_{ij}\varepsilon_{ij}$ term represents the energy density of the stress/strain field. In an attempt to model the synthesis of the shell, the deposition of atoms onto the nanowire surface is assumed to proceed at a fixed rate Q in atoms per unit

area and unit time. Considering the continuity equation, one can show that to first order in δ the radial component of a vector $\mathbf{R}_s$ to a point on the surface will change with time as [26]

$$\dot{R}_s = \Omega Q + \frac{D_s \Gamma \Omega^2}{kT} \Delta_s \left(\gamma \kappa + \frac{1}{2} \sigma_{ij} \varepsilon_{ij} \right)_{r=R_s} \tag{5.48}$$

Here, Δ_s denotes the surface Laplacian. Since all terms in parentheses in Eq. (5.48) are at least of order δ, it is sufficient to use the zeroth-order approximation for the Laplacian Δ_s [26].

$$\Delta_s^0 = \frac{1}{R_2^2} \partial_\phi^2 + \partial_z^2 \tag{5.49}$$

Using the same argument, that is, that we are only interested in first-order contributions, one can evaluate the expression in parentheses at R_2 instead of R_s. Equation (5.48) then becomes

$$\dot{R}_s = \Omega Q + \frac{D_s \Gamma \Omega^2}{kT} \Delta_s^0 (\gamma \kappa + \bar{\sigma}_{ij} \tilde{\varepsilon}_{ij})_{r=R_2} \tag{5.50}$$

Furthermore, one can show that $\tilde{\varepsilon}_{ij}$ is proportional to $\delta \cos(qz)\cos(n\phi)$ [26]. Inserting the explicit forms of κ, performing Δ_s^0, and separating the terms proportional to the cosines from those that are not, one can find that

$$\dot{R}_2 = \Omega Q \tag{5.51}$$

$$\dot{\delta} = \frac{D_s \Gamma \Omega^2 \gamma}{kT} S \delta \tag{5.52}$$

So the radius R_2 of the shell grows at a rate that is equal to the deposition rate as expected. The time dependence of the amplitude δ of a perturbation is governed by a simple differential equation indicating an exponential time dependence

$$\delta(t) = \delta_0 \exp\left(\frac{D_s \Gamma \Omega^2 \gamma}{kT} S t \right) \tag{5.53}$$

with δ_0 being the amplitude of the perturbation at $t = 0$. The stability parameter S is given by

$$S = \left(\frac{n^2}{R_2^2} + q^2 \right) \left(\frac{1 - n^2}{R_2^2} - q^2 - \frac{\bar{\sigma}_{ij} \tilde{\varepsilon}_{ij}}{\gamma} \right) \tag{5.54}$$

and it is this parameter that determines the magnitude and sign of the exponent. This exponential time dependence according to Eq. (5.53) leads to an increase of δ if $S > 0$. That means that the surface is unstable with respect to this particular perturbation, as the amplitude of the perturbation will grow exponentially. For $S < 0$, the initial amplitude of perturbation decays exponentially with time and the cylindrical surface is said to be stable with respect to this particular perturbation. The upcoming task is to

sort out those perturbations with the greatest positive value of S, as they are most critical for the roughening of the shell.

5.4.4 Results and Discussion

We have seen that the exponential behavior of δ depends on the sign and magnitude of the stability parameter S. To give an impression of how the stability parameter S generally behaves, S is shown in Figure 5.4 as a function of q for the first six modes of a Ge nanowire of 10 nm radius covered by a 1 nm thick Si shell. The surface free energy is assumed to be $\gamma = 1.5\,\mathrm{J/m^2}$ and the surface stress $\tau = 1.0\,\mathrm{N/m}$ [50, 51]. The first thing to notice in Figure 5.4 is that (going from left to right) the stability parameter S of $n = 0$ is zero in the limit $q \to 0$, then exhibits a maximum, and finally becomes negative for large values of q. This behavior is quite analogous to what has been found by Spencer *et al.* [25] considering semi-infinite substrates. For this mode and wavenumbers $q < 0.37\,\mathrm{nm^{-1}}$, S is positive, so the amplitude of the perturbation would grow exponentially, corresponding to a roughening of the surface. Just as an aside, it is interesting to note that the $n = 0$ mode exhibits positive values of S even for vanishing misfit. In this case, the maximum of S is located at about $2\pi\sqrt{2}R_2$, which corresponds to the wavelength of the classical, surface stress-driven Plateau–Rayleigh instability [52, 53].

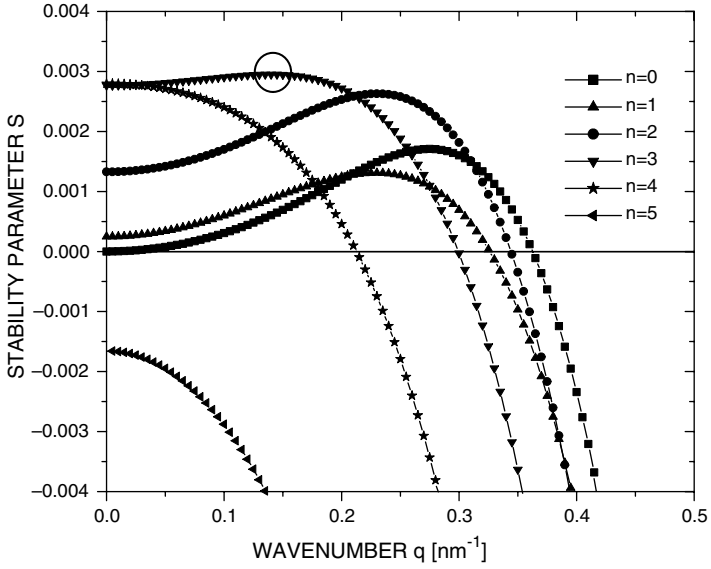

Figure 5.4 Stability parameter S as a function of the wavenumber q for $R_1 = 10\,\mathrm{nm}$, $R_2 = 11\,\mathrm{nm}$, $G = 46\,\mathrm{GPa}$, $\nu = 0.26$, $m = -0.043$, $\tau = 1.0\,\mathrm{N/m}$, and $\gamma = 1.5\,\mathrm{J/m^2}$.

Furthermore, one can see in Figure 5.4 that all modes with $n \leq 4$ do have positive values of S for certain wavenumbers q, ranging from $q = 0$ to about $q \approx 0.3\,\mathrm{nm}^{-1}$. Thus, the surface of such a core–shell nanowire would be unstable for the first four modes and wavelengths (in z-direction) longer than roughly the diameter of the nanowire. Owing to the exponential time dependence of δ on S, the perturbation with the greatest S value will grow the fastest. In case of the nanowire considered in Figure 5.4, this is the $n = 3$ mode that exhibits a maximum at about $q \approx 0.16\,\mathrm{nm}^{-1}$ (marked by a circle in Figure 5.4) corresponding to a wavelength of about $4R_2$. This will be called the fastest growing mode. This fastest growing mode is characterized by its wavenumber q_{fg}, wavenumber n_{fg}, and the stability parameter S_{fg}. Owing to exponential time dependence of δ, one may assume that the fastest growing mode will dominate the other perturbation modes after a while, so that the fastest growing mode determines the final morphology of the shell. Therefore, in the following discussion, we will mainly concentrate on the properties of the fastest growing mode and, in particular, on the dependence of S_{fg} and n_{fg} on parameters such as the core radius or the shell thickness.

First, let us examine the properties of n_{fg}, shown in Figure 5.5a, as a function of the core radius R_1 for various shell thicknesses ranging from 1 to 7 nm. The misfit parameter is taken to be $m = -0.044$, corresponding to the misfit of a Ge-core–Si-shell nanowire. One can see in Figure 5.5a that the mode number n_{fg} of the fastest growing mode increases strongly for increasing core radius and decreasing shell thickness. So one can expect that roughening, in particular for the initial phase of shell growth on rather thick nanowires, will show a quite complex behavior. At larger shell thicknesses, modes with lower mode number should become dominant. It is also interesting to note that the question which modes become dominant strongly depends on the sign of the misfit. Assuming a positive surface stress τ and a negative misfit m, one can show that due to the surface stress, modes with large surface

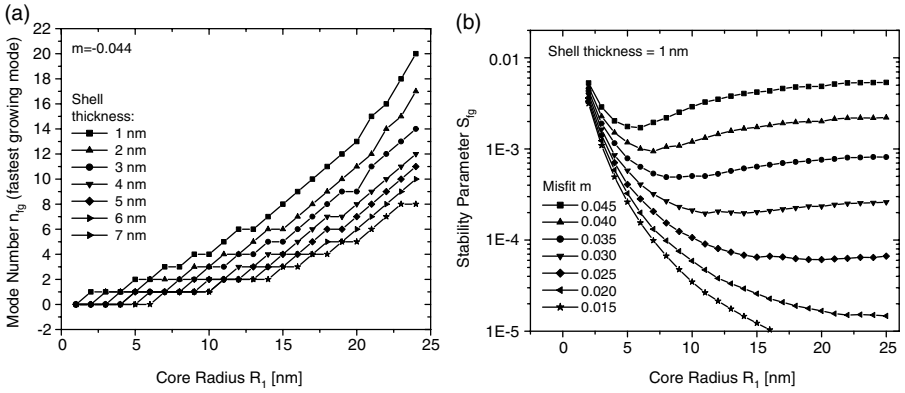

Figure 5.5 (a) n_{fg} as a function of the core radius R_1 for $m = -0.044$ and various shell thicknesses, $\tau = 1.0\,\mathrm{N/m}$. (b) Stability parameter (S_{fg}) as a function of the core radius R_1 for various misfit parameters m, $\tau = 0\,\mathrm{N/m}$. $G = 46\,\mathrm{GPa}$, $\nu = 0.26$, and $\gamma = 1.5\,\mathrm{J/m^2}$.

curvature, that is, large wavenumber n, are favored (in the sense of greater S) [26], whereas for positive values of m, the opposite is the case. For positive misfits, surface stress reduces the magnitude of the stability parameter of high-n modes. Thus, one can expect that for a positive surface stress, thin Ge-core–Si-shell nanowires will show a more complex roughening behavior than Si-core–Ge-shell nanowires. For positive m, it is in fact often the $n = 0$ mode that grows the fastest.

The dependence of the stability parameter S_{fg} of the fastest growing mode on the core radius R_1 is displayed in Figure 5.5b for various misfits m and a fixed shell thickness of 1 nm. It is evident that S_{fg} depends quite strongly on the misfit m as expected. Furthermore, what is interesting to note is that for large misfits, for example, $m = 0.045$, the curve exhibits a minimum at a core radius of about 6 nm. This means that from a surface stability point of view, it is advantageous to choose such a core radius if smooth, nonroughened core–shell nanowires are to be synthesized. Figure 5.6a and b shows S_{fg} as a function of the core radius for various shell thicknesses. Again, surface stress is $\tau = 1.0\,\mathrm{N/m}$. Figure 5.6a, with a misfit $m = +0.044$, approximately corresponds to the case of a Si-core–Ge-shell nanowire (Figure 5.6b), with $m = -0.044$ to a Ge-core–Si-shell nanowire. The first apparent feature of Figure 5.6 is the strong dependence on the shell thickness. In both cases, $m = +0.044$ and $m = -0.044$, an increase in the shell thickness from 1 to 7 nm leads to a decrease in S_{fg} by more than one order of magnitude—more or less independent of the core radius. Concerning the overall stability, one therefore has to conclude that the initial phase of growth, where the shell is thinnest, is most critical with respect to a roughening of the surface. For experimentalists, this signifies that extreme care should be taken in the initial phase of shell growth. To reduce the roughening tendency, it might be advisable to synthesize a graded junction in the initial phase of shell growth. This can be, considering a Ge-core–Si-shell nanowire, for example, be easily done be steadily reducing the Ge content in the initial phase of

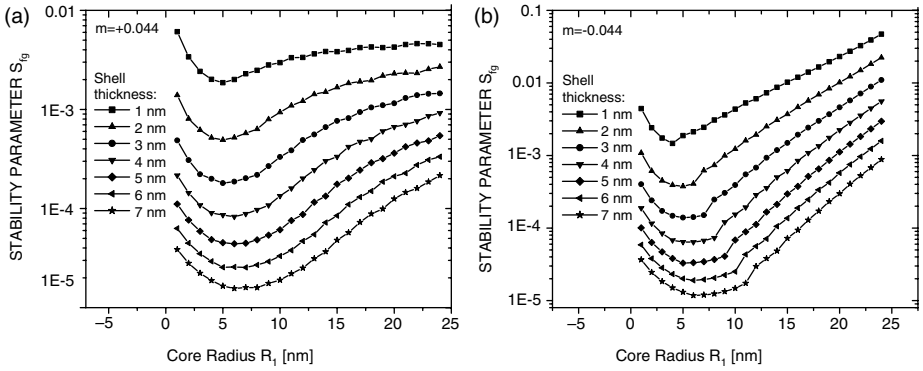

Figure 5.6 Stability parameter (S_{fg}) for various shell thicknesses as a function of the core radius R_1 using $G = 46\,\mathrm{GPa}$, $\nu = 0.26$, $\tau = 1.0\,\mathrm{N/m}$, and $\gamma = 1.5\,\mathrm{J/m^2}$; (a) $m = +0.044$ (Si-core–Ge-shell) and (b) misfit $m = -0.044$ (Ge-core–Si-shell).

shell growth. The most interesting feature, visible in Figure 5.6a and b, is the pronounced minimum one can find at a core radius of 5 nm. This means that one way of reducing the tendency for roughening is to use nanowires with diameter of about 10 nm as a starting material for the core–shell structure. By reducing the diameter from 50 to 10 nm, R_1, the stability parameter of a Ge-core–Si-shell nanowire (see Figure 5.6b), is reduced by more than one order of magnitude, which means a significant increase in surface stability.

Within the framework of the model, it could be shown that the surface is most unstable when the shell thickness is of the order of 1 nm or less. Consequently, it is the initial phase of shell growth that would be most sensitive to a roughening of the surface. In addition, the model shows that for $m \gtrsim 0.03$, there exists a core radius of maximum stability, which means that synthesizing cylindrical core–shell nanowires should be easiest for core diameters of about 10 nm.

5.5 Conclusion

The main conclusion of considering dislocation formation in both axial and core–-shell nanowires is that the critical misfit, up to which dislocation-free nanowires can be synthesized, is strongly radius dependent and it increases with decreasing radius. This is mainly a scaling effect. By reducing the radius of the nanowires, the strain energy stored in the system changes proportionally to the volume of the system. Moreover, if the volume is small enough, at some point the energy stored will not suffice anymore to induce the formation of a dislocation. Therefore, reducing the radius helps to prevent dislocation formation. Concerning the strain-induced roughening instability of shell, one must conclude that, in contrast to dislocation formation, this relaxation mechanism does not vanish at smaller radii. Nevertheless, reducing the radius might still be beneficial to increase the stability of the system.

Acknowledgements

This work was supported by the joint Fraunhofer–Max Planck project *nanoSTRESS*.

References

1 Schmidt, V., Wittemann, J.V., and Gösele, U. (2010) Growth, thermodynamics, and electrical properties of silicon nanowires. *Chem. Rev.*, **110**, 361–388.

2 Wu, Y., Fan, R., and Yang, P. (2002) Block-by-block growth of single-crystalline Si/SiGe superlattice nanowires. *Nano Lett.*, **2** (2), 83.

3 Redwing, J.M., Lew, K.K., Bogart, T.E., Pan, L., Dickey, E.C., Carim, A.H., Wang, Y., Cabassi, M.A., and Mayer, T.S. (2004) Synthesis and properties of Si and SiGe/Si nanowires. *Proc. SPIE*, **5361**, 52.

4 Hanke, M., Eisenschmidt, C., Werner, P., Zakharov, N.D., Syrowatka, F., Heyroth, F., Schäfer, P., and Konovalov, O. (2007) Elastic strain relaxation in axial

Si/Ge whisker heterostructures. *Phys. Rev. B*, **75**, 161303.

5 Dujardin, R., Poydenot, V., Devillers, T., Favre-Nicolin, V., Gentile, P., and Barski, A. (2006) Growth mechanism of Si nanowhiskers and SiGe heterostructures in Si nanowhiskers: X-ray scattering and electron microscopy investigations. *Appl. Phys. Lett.*, **89**, 153129.

6 Zakharov, N.D., Werner, P., Gerth, G., Schubert, L., Sokolov, L., and Gösele, U. (2006) Growth phenomena of Si and Si/Ge nanowires on Si(111) by molecular beam epitaxy. *J. Cryst. Growth*, **290**, 6.

7 Clark, T.E., Nimmatoori, P., Lew, K.K., Pan, L., Redwing, J.M., and Dickey, E.C. (2008) Diameter dependent growth rate and interfacial abruptness in vapor–liquid–solid $Si/Si_{1-x}Ge_x$ heterostructure nanowires. *Nano Lett.*, **8** (4), 1246.

8 Lauhon, L.J., Gudiksen, M.S., Wang, D., and Lieber, C.M. (2002) Epitaxial core–shell and core–multishell nanowire heterostructures. *Nature*, **420**, 57.

9 Xiang, J., Lu, W., Hu, Y., Wu, Y., Yan, H., and Lieber, C.M. (2006) Ge/Si nanowire heterostructures as high-performance field-effect transistors. *Nature*, **441**, 489.

10 Asaro, R.J. and Tiller, W.A. (1972) Interface morphology development during stress corrosion cracking: part I. Via surface diffusion. *Metall. Trans.*, **3**, 1789–1796.

11 Grinfeld, M.A. (1986) Instability of the separation boundary between a non-hydrostatically stressed elastic body and a melt. *Sov. Phys. Dokl.*, **31** (10), 831–834.

12 Stangl, J., Holý, V., and Bauer, G. (2004) Structural properties of self-organized semiconductor nanostructures. *Rev. Mod. Phys.*, **76** (3), 725.

13 Tersoff, J. and LeGoues, F.K. (1994) Competing relaxation mechanisms in strained layers. *Phys. Rev. Lett.*, **72** (22), 3570.

14 Wagner, R.S. and Ellis, W.C. (1965) The vapor–liquid–solid mechanism of crystal growth and its application to silicon. *Trans. Metall. Soc. AIME*, **233**, 1053.

15 Ertekin, E., Greaney, P.A., Sands, T.D., and Chrzan, D.C. (2003) Equilibrium analysis of lattice-mismatched nanowire heterostructures. *Mater. Res. Soc. Symp. Proc.*, **737**, F10.4.1.

16 Kästner, G. and Gösele, U. (2004) Stress and dislocations at cross-sectional heterostructures in a cylindrical nanowire. *Philos. Mag.*, **84** (35), 3803.

17 Ertekin, E., Greaney, P.A., Chrzan, D.C., and Sands, T.D. (2005) Equilibrium limits of coherency in strained nanowire heterostructures. *J. Appl. Phys.*, **97**, 114325.

18 Glas, F. (1997) Thermodynamics of a stressed alloy with a free surface: coupling between the morphological and compositional instabilities. *Phys. Rev. B*, **55** (17), 11277–11286.

19 Lee, M.L., Fitzgerald, E.A., Bulsara, M.T., Currie, M.T., and Lochtefeld, A. (2005) Strained Si, SiGe, and Ge channels for high-mobility metal–oxide–semiconductor field-effect transistors. *J. Appl. Phys.*, **97**, 011101.

20 Schmidt, V., Riel, H., Senz, S., Karg, S., Riess, W., and Gösele, U. (2006) Realization of a silicon nanowire vertical surround-gate field-effect transistor. *Small*, **2** (1), 85.

21 Liang, Y., Nix, W.D., Griffin, P.B., and Plummer, J.D. (2005) Critical thickness enhancement of epitaxial SiGe films grown on small structures. *J. Appl. Phys.*, **97**, 043519.

22 Srolovitz, D.J. (1989) On the stability of surfaces of stressed solids. *Acta Metall.*, **37** (2), 621–625.

23 Gao, H. and Nix, W.D. (1999) Surface roughening of heteroepitaxial thin films. *Annu. Rev. Mater. Sci.*, **29**, 173.

24 Spencer, B.J., Voorhees, P.W., and Davis, S.H. (1991) Morphological instability in epitaxially strained dislocation-free solid films. *Phys. Rev. Lett.*, **67** (26), 3696–3699.

25 Spencer, B.J., Voorhees, P.W., and Davis, S.H. (1993) Morphological instability in epitaxially strained dislocation-free solid films: linear stability theory. *J. Appl. Phys.*, **73** (10), 4955–4970.

26 Schmidt, V., McIntyre, P.C., and Gösele, U. (2008) Morphological

instability of misfit-strained core–shell nanowires. *Phys. Rev. B*, **77**, 235302.
27 Kirill, D.J., Davis, S.H., Miksis, M.J., and Vorhees, P.W. (1999) *Proc. R. Soc. Lond. A*, Morphological instability of a whisker. **455** (1990), 3825–3844.
28 Colin, J., Grilhé, J., and Junqua, N. (1997) Surface instabilities of a stressed cylindrical whisker. *Philos. Mag. A*, **76** (4), 793.
29 Pan, L., Lew, K.K., Redwing, J.M., and Dickey, E.C. (2005) Stranski–Krastanow growth of germanium and silicon nanowires. *Nano Lett.*, **5** (6), 1081–1085.
30 Mullins, W.W. (1957) Theory of thermal grooving. *J. Appl. Phys.*, **28** (3), 333–339.
31 Landau, L.D. and Lifshitz, E.M. (1986) Theory of elasticity, in *Course of Theoretical Physics*, vol. 7, 3rd edn, Elsevier, Oxford, Chapter 1, pp. 1–36.
32 Gibbs, J.W. (1906). *The Scientific Papers of J. Williard Gibbs, Vol. I: Thermodynamics*, Longmans, Green & Company, London, Chapter 3, pp. 315–318.
33 Shuttleworth, R. (1950) The surface tension of solids. *Proc. Phys. Soc. A*, **63** (5), 444.
34 Cahn, J.W. (1980) Surface stress and the chemical equilibrium of small crystals I. the case of the isotropic surface. *Acta Metall.*, **28**, 1333–1338.
35 Alerhand, O.L., Vanderbilt, D., Meade, R.D., and Joannopoulos, J.D. (1988) Spontaneous formation of stress domains on crystal surfaces. *Phys. Rev. Lett.*, **61** (17), 1973–1976.
36 Middel, M.T., Zandvliet, H.J.W., and Poelsema, B. (2002) Surface stress anisotropy of Ge(001). *Phys. Rev. Lett.*, **88** (19), 196105.
37 Métois, J.J., Saúl, A., and Müller, P. (2005) Measuring the surface stress polar dependence. *Nat. Mater.*, **4**, 238–242.
38 Payne, M.C., Roberts, N., Needs, R.J., Needels, M., and Joannopoulos, J.D. (1989) Total energy and stress of metal and semiconductor surfaces. *Surf. Sci.*, **211–212**, 1–20.
39 Meade, R.D. and Vanderbilt, D. (1989) Origins of stress on elemental and chemisorbed semiconductor surfaces. *Phys. Rev. Lett.*, **63** (13), 1404–1407.
40 Sato, H. and Yagi, K. (1993) Surface stress on Si(001) 2×1 surfaces studied by TEM. *J. Phys. Condens. Matter*, **5**, 2095–2100.
41 Twesten, R.D. and Gibson, J.M. (1994) Measurement of Si(111) surface stress by a microscopic technique. *Phys. Rev. B*, **50** (23), 17628–17631.
42 Meade, R.D. and Vanderbilt, D. (1989) Adatoms on Si(111) and Ge(111) surfaces. *Phys. Rev. B*, **40** (6), 3905–3913.
43 van Heys, J. and Pehlke, E. (2005) Surface stress of partially H-covered Si(001) surfaces. *Phys. Rev. B*, **72**, 125351.
44 Papkovich, P.F. (1932) The representation of the general integral of the fundamental equations of elasticity theory in terms of harmonic functions. *Izv. Acad. Nauk SSR Ser. Fiz. Mat. Nauk*, **10**, 1425.
45 Neuber, H. (1934) Ein neuer ansatz zur lösung räumlicher probleme der elastitätstheorie. *Z. Angew. Math. Mech.*, **14**, 203–212.
46 Sadd, M.H. (2005) *Theory, Applications and Numerics*, Elsevier, New York, Chapter 13, pp. 347–358.
47 Alexander, J.I.D. and Johnson, W.C. (1985) Thermomechanical equilibrium in solid-fluid systems with curved interfaces. *J. Appl. Phys.*, **58** (2), 816–824.
48 Larché, F.C. and Cahn, J.W. (1985) The interactions of composition and stress in crystalline solids. *Acta Metall.*, **33** (3), 331–357.
49 Leo, P.H. and Sekerka, R.F. (1989) The effect of surface stress on crystal-melt and crystal-crystal equilibrium. *Acta Metall.*, **37** (12), 3119–3138.
50 Jaccodine, R.J. (1963) Surface energy of germanium and silicon. *J. Electrochem. Soc.*, **110** (6), 524.
51 Zhang, J.M., Ma, F., Xu, K.W., and Xin, X.T. (2003) Anisotropy analysis of the surface energy of diamond cubic crystals. *Surf. Interface Anal.*, **35**, 805.
52 Plateau, M.T. (1856) On the recent theories of the constitution of jets of liquid issuing from circular orifices. *Philos. Mag.*, **12**, 286.
53 Rayleigh, L. (1878) On the instability of jets. *Proc. Lond. Math. Soc.*, **s1–s10** (1), 4–13.